Thermodynamic Insights on Desalination Processes: Exergy Analysis, Minimum Separation Work, and Advances in Capacitive Deionization with Battery Electrode

Ayoub TAKTOUR[1], Abderrahman MELLALOU[1], Abdelkader OUTZOURHIT[1], Fouad GHAMOUSS[1].

[1] Materials Science, Energy, and Nano-engineering Department, Mohammed VI Polytechnic University, Ben Guerir, Morocco

Supporting information

Crafting a high-quality review paper constitutes a crucial phase in a research project, serving to elucidate the existing state of knowledge, reconcile apparent contradictions, pinpoint areas requiring further investigation, and establish consensus in situations where none was previously present [1].

B Overview of Exergy variation in desalination technologies

the mathematical representation of exergy, denoted as e, is as follows:[2]

$$e = (u - u^*) + p_0(v - v^*) - T_0(s - s^*) + \sum_{i=1}^{n} x_i(\mu_i^* - \mu_{i,0})/M_i \quad (1)$$

In the given expressions, where u, v, s, m, and x represent specific internal energy, specific volume, specific entropy, chemical potential, and mass fraction, respectively. The properties denoted with **(*)** in the equation are evaluated at the temperature and pressure of the environment, maintaining the same composition or concentration as the initial state. This condition is known as the restricted dead state, where only temperature and pressure are adjusted to match environmental values. Conversely, properties denoted with **(0)** in the equation are determined at the temperature, pressure, and concentration of the environment, referred to as the global dead state.

In the initial scenario where $P = P_0 \, and \, x = x_0$, the chemical exergy (represented as the last term in Eq (1)) becomes zero. The exergy expression for an ideal gas mixture can then be formulated as follows:

$$e = c_v(T - T_0) + p_0\left(\frac{RT}{p} - \frac{RT_0}{p_0}\right) - T_0\left[c_p ln\left(\frac{T}{T_0}\right) - R ln\left(\frac{p}{p_0}\right)\right] \quad (2)$$

$(P = P_0)$

$$e = c_v(T - T_0) + R(T - T_0) - T_0 c_p ln\left(\frac{T}{T_0}\right) \quad (3)$$

With $(c_p = c_v + R)$

$$e = c_p T_0\left[\frac{T}{T_0} - ln\left(\frac{T}{T_0}\right) - 1\right] \quad (4)$$

In the second scenario where $T = T_0 \, and \, x = x_0$, the same as before the chemical exergy term becomes zero and the exergy can be written for an ideal gas mixture as

$$e = c_v(T - T_0) + p_0\left(\frac{RT}{p} - \frac{RT_0}{p_0}\right) - T_0\left[c_p \ln\left(\frac{T}{T_0}\right) - R\ln\left(\frac{p}{p_0}\right)\right] \quad (5)$$

$(T = T_0)$, thus

$$e = RT_0\left[\frac{p_0}{p} + ln\left(\frac{p}{p_0}\right) - 1\right] \quad (6)$$

In the third scenario where $T = T_0 \, and \, P = P_0$, the initial two terms in the exergy equation (as per Eq (1)) disappear. The sole remaining term is the final one, representing chemical exergy. The exergy in this instance can be expressed as follows:

$$e = \sum_{i=1}^{n} x_i\left(\mu_i^* - \mu_i^0\right) \quad (7)$$

In the context of an optimal blend model or an ideal mixture model, the disparities in chemical potential are expressed as.

$$e = \sum_{i=1}^{n} x_i R_i T ln\left(\frac{x_i}{x_{i,0}}\right) \quad (8)$$

Assuming a mixture composed of two substances leads to the following.

$$e = x_1 R_1 T_0 ln\left(\frac{x_1}{x_{1,0}}\right) + x_2 R_2 T_0 ln\left(\frac{x_2}{x_{2,0}}\right) \quad (9)$$

Additionally, it is within our knowledge that $(x_1 = 1 - x_2)$ and $(x_{1,0} = 1 - x_{2,0})$

$$e = RT_0\left[(1-x) ln\left(\frac{1-x}{1-x_0}\right) + x ln\left(\frac{x}{x_0}\right)\right] \quad (10)$$

C Separation and Mixing in Desalination

Considering two ideal gases separated by a physical barrier in a container.

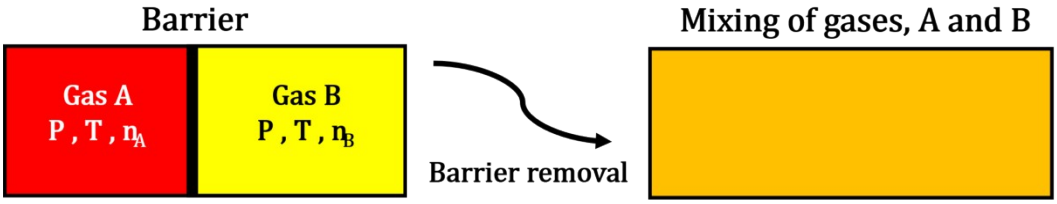

Figure 1 Schematic illustration of the mixing of two gases

$$G = \sum_j n_j \mu_j \qquad (11)$$

$$G^i = n_A \mu_A^i + n_B \mu_B^i \quad ; \quad G^f = n_A \mu_A^f + n_B \mu_B^f \quad (12)$$

As $\Delta G_{mix} = (G^f - G^i)$, the change in free energy is given by:

$$\Delta G_{mix} = n_A\left(\mu_A^f - \mu_A^i\right) + n_B\left(\mu_B^f - \mu_B^i\right) \qquad (13)$$

We need to recall $\left(\frac{\partial \mu_j}{\partial P}\right)_T = V_{m,j}$, molar volume.

$$d\mu_j = V_{m,j} dP \quad (14)$$

Form Eq (4), the following can be written.

$$d\mu_j = RT\frac{dP}{P} \quad (15)$$

$$\int_{\mu_j^i}^{\mu_j^f} d\mu_j = RT \int_{P}^{P_j} \frac{dP}{P} \quad (16)$$

$$\mu_j^f - \mu_j^i = RT\, ln(\frac{P_j}{P}) \quad (17)$$

Thus

$$\Delta G_{mix} = n_A RT ln\left(\frac{P_A}{P}\right) + n_B RT ln\left(\frac{P_B}{P}\right) \quad (18)$$

According to Dalton`s law $(\frac{P_j}{P} = x_j)$ and, as $(n_j = n x_j)$ hence:

$$\Delta G_{mix} = n_A RT ln x_A + n_B RT ln x_B \quad (19)$$

$$\Delta G_{mix} = nRT\left(x_A ln(x_A) + x_B ln(x_B)\right) \quad (20)$$

Where, R is the gas constant $(8.314\,J/(mol{\cdot}K)$, T is the temperature in Kelvin, x_A and x_B are the mole fractions of the two components in the solution. This equation describes the free energy change associated with the mixing of two components in an ideal solution. If ΔG_{mix} is negative, it suggests that the mixing is favorable. For the case of desalination, particularly in the context of water desalination, it typically involves the separation of salt (solute) from water (solvent). The process of desalination often requires energy input, and the Gibbs free energy is a thermodynamic parameter that provides insights into the spontaneity of the process. In the context of desalination, the Gibbs free energy change ΔG_{mix} can be related to the work done W by the equation:

$$\Delta G_{mix} = W_{non-PV} \quad (21)$$

where W_{non-PV} is the non-pressure-volume work associated with the process. This work is required to overcome the thermodynamic barrier for separating solute from the solvent. In desalination processes such as reverse osmosis or distillation, the reduction in ΔG_{mix} is achieved by applying external energy, often in the form of pressure or heat, to drive the separation. The specifics of the equations involved would depend on the particular desalination process under consideration. Consequently, when examining the Gibbs free energy of mixing in the context of an ideal two-component solution, and specifically in relation to desalination processes, certain considerations come into play.

$$\Delta_{mix}G = nRT\left[\mathrm{x}_S \ln\left(x_S\right) + x_W ln(x_W)\right] \quad (22)$$

x_W molar fraction of Water x_S molar fraction of Salt $x_W = 1 - x_S$

$$\Delta_{mix}G = nRT\left[\mathrm{x}_S \ln\left(x_S\right) + (1 - x_S)\ln\left(1 - x_S\right)\right] \quad (23)$$

with Taylor series expansion and dilute solution approximation (i.e., $xs \ll 1$) using $\ln(1 - xs) \approx xs$ to yield.

$$\Delta_{mix}G \approx nRTx_S\left[\ln\left(x_S\right) - 1\right] \quad (24)$$

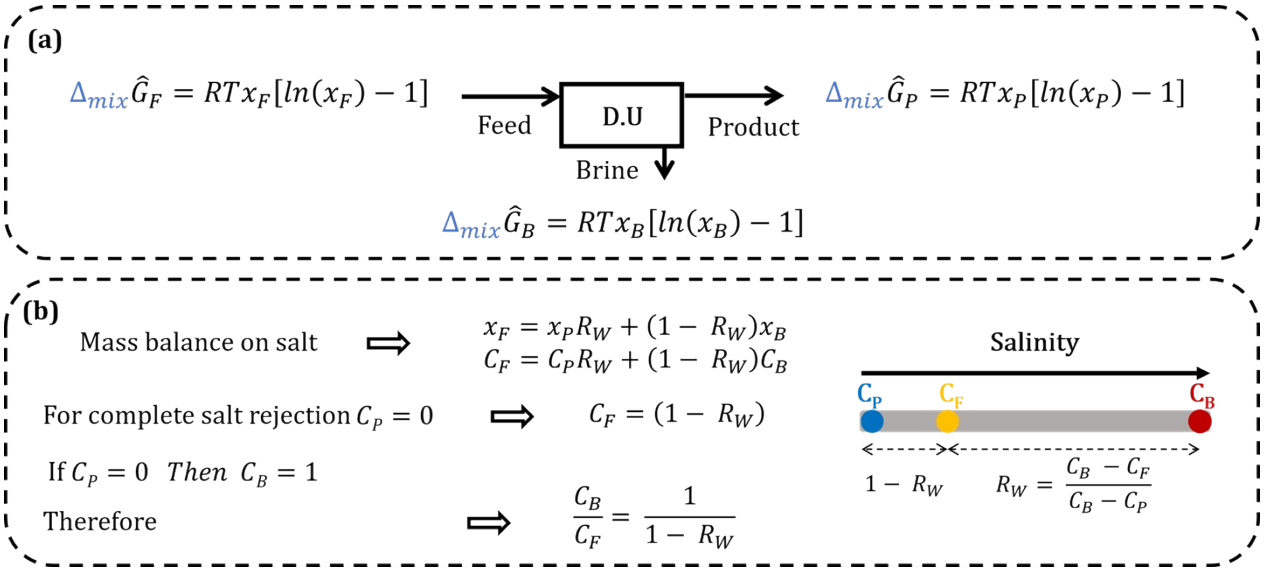

Figure 2 (a) The primary streams of a desalination unit, (b) Mass balance on salt for desalination process

The Gibbs free energy of separation for a desalination process:

$$\Delta_{sep}G = \Delta_{mix}G_P + \Delta_{mix}G_B - \Delta_{mix}G_F \quad (25)$$

$$\Delta_{sep}\hat{G} = R_W\Delta_{mix}\hat{G}_P + (1 - R_W)\Delta_{mix}\hat{G}_B - \Delta_{mix}\hat{G}_F \quad (26)$$

Specific energy consumption (SEC) is defined as

$$SEC_{min} = \frac{\Delta_{sep}\hat{G}}{R_W\hat{V}_w} = \frac{R_W\Delta_{mix}\hat{G}_P + (1 - R_W)\Delta_{mix}\hat{G}_B - \Delta_{mix}\hat{G}_F}{R_W\hat{V}_w} \quad (27)$$

$$SEC_{min} = \frac{RT}{\hat{V}_w}\left[\frac{x_F}{R_W}\ln\left(\frac{x_B}{x_F}\right) - x_P ln\left(\frac{x_B}{x_P}\right)\right] \quad (28)$$

Using $x_s = \nu C_s\hat{V}_w$, where ν is the number of dissociated ions per salt molecule $(2\ for\ NaCl)$

$$SEC_{min} = 2RT\left[\frac{C_F}{R_W}ln\left(\frac{C_B}{C_F}\right) - C_P ln\left(\frac{c_B}{c_P}\right)\right] \quad (29)$$

For complete salt rejection $C_P = 0$, and the van't Hoff relation $\pi_f = 2RTC_f$

$$SEC_{min} = \frac{2RTC_F}{R_W}ln\left(\frac{C_B}{C_F}\right) \quad (30)$$

$$SEC_{min} = -\frac{\pi_F}{R_W}\ln(1 - R_W) \quad (31)$$

The SEC_{min} is determined only by the feed Osmotic Pressure $\pi_f$and water Recovery Ratio R_W.

Thermodynamic energy efficiency (TEE) is defined as:

$$TTE = \frac{\Delta G_{mix}}{SEC_{min}} = \frac{\Delta G_{ion}}{SEC_{ion}} \quad (32)$$

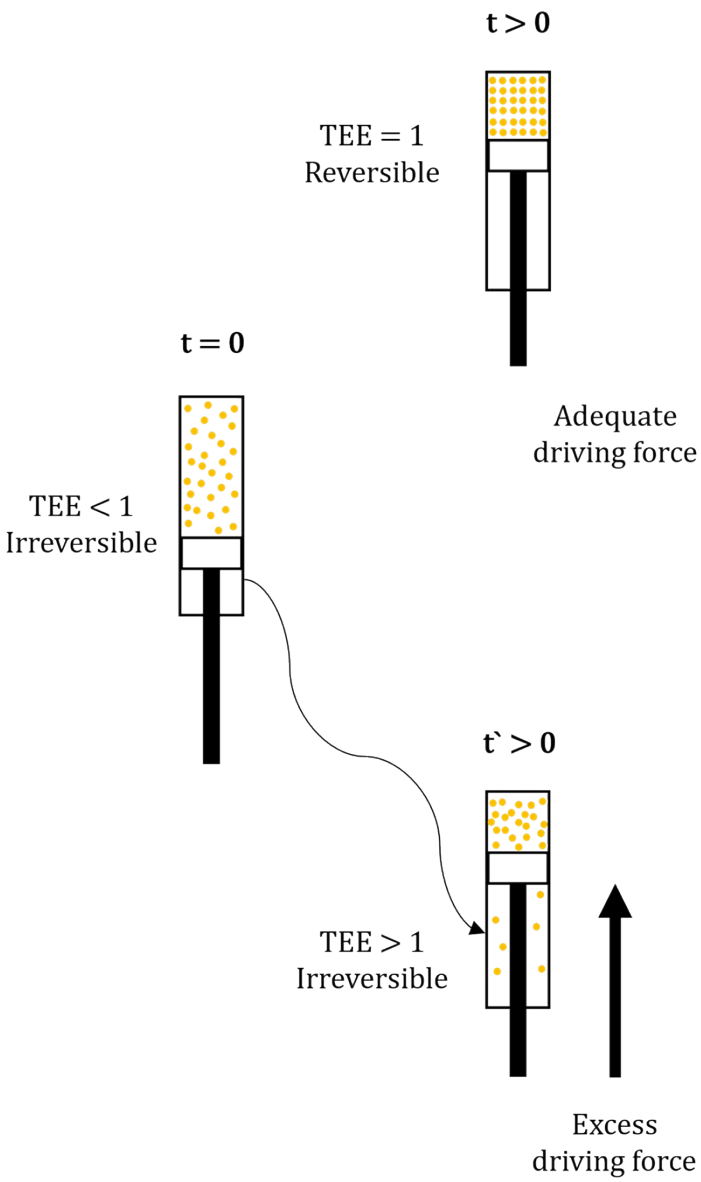

Figure 3 illustration of TEE

Desalination technologies data

Distillation

Table 1 Distillation data

C_0 (mM)	R_w (%)	ΔG_W (Wh/m^3)	SEC (Wh/m^3)	TEE (%)	Rf
657	28	1093.3	24786	4.4	[3]
717	40	1280.7	14659.5	8.7	[4]
846	9	1249.6	16791.3	7.4	[4]
682	6	993.7	19906.5	5	[5]
768	14	1178.3	14493.2	8.1	[6]
700	50	1396.3	20566.4	6.8	[7]
879	8	1301.8	18194.3	7.2	[8]
768	18	1223.6	13398.8	9.1	[9]
717	41	1263.5	17207.3	7.3	[10]
717	38	1232.1	15881.8	7.8	[10]
717	39	1244.8	17240.4	7.2	[11]
768	28	1267.5	18965.4	6.7	[11]
768	17	1164	10206.3	11.4	[11]
665	40	1208.8	22769.3	5.3	[12]
109	31	173.8	17827.7	1	[13]
597	21	920	9289.3	9.9	[14]
597	33	999.7	10797.5	9.3	[15]
699	48	1305.6	6354.9	20.5	[15]
61	70	1449.5	24684.8	5.9	[16]
61	55	1222	13272.3	9.2	[17]
67	40	1208.9	23791.6	5.1	[18]
72	34	1249.1	12585.1	9.9	[19]
11	98	632.7	22145.6	2.9	[13]
60	33	1027.3	26498.1	3.9	[13]
82	16	1256.4	34048.8	3.7	[20]
68	29	1223.4	15478.2	7.9	[17]
72	30	1296.9	14310.9	9.1	[11]
77	15	1181.5	7756.5	15.2	[6]
72	33	1200.5	12546	9.6	[21]
89	29	1478.7	17751.1	8.3	[22]
76	40	1363.8	21834	6.2	[23]
648	40	1123.3	11501	9.8	[24]
512	90	1802.3	26587	6.8	[25]
717	40	1243.2	9400	13.2	[24]
717	10	1072.6	11800	9.1	[19]

Reverse osmosis (RO)

Table 2 Reverse osmosis data

C_0 (mM)	Rw (%)	ΔG_W (Wh/m^3)	SEC (Wh/m^3)	TEE (%)	Rf
11	70	26	228	11.4	[26]
8	65	18	119	15.3	[26]
15	75	39	322	12.1	[26]
15	75	39	264	14.8	[26]
43	13	64	139	46	[27]
43	23	68	133	50.7	[27]
51	81	145	556	26.1	[28]
34	79	93	378	24.6	[28]
15	75	37	333	11.2	[29]
43	66	96	389	24.7	[30]
60	75	152	472	32.3	[31]
712	45	1302	1806	72.1	[32]
698	45	1276	1769	72.1	[32]
602	28	972	1578	61.6	[33]
841	13	1239	1717	72.2	[33]
975	20	1447.1	1772.2	81.65	[34]
686	45	1217.2	1750	69.56	[35]
624	50	1140.8	1611.1	70.81	[36]
659	40	1133.1	1811.1	62.56	[34]
677	28	1051.3	1638.9	64.15	[37]
677	25	997.9	1972.2	50.6	[37]
568	40	936.8	1622.2	57.75	[33]
196	34	312.6	583.3	53.59	[38]
257	65	259.6	583.3	44.51	[39]
80	72	157.3	333.3	47.2	[40]
51	81	128.1	555.6	23.07	[28]
68	50	120.1	416.7	28.81	[41]
91	50	116	416.7	27.85	[42]
39	75	94.7	833.4	11.37	[43]
42	71	90.5	394.5	22.95	[30]
34	79	89.7	377.8	23.74	[28]
62	23	88.5	133.3	66.38	[27]
62	13	85.2	138.9	61.31	[27]
34	75	78.8	377.8	20.85	[44]
46	67	71.7	416.7	17.21	[42]
60	12	63	611	10.3	[31]
17	68	34.8	333.4	10.45	[41]

13	75	31.9	322.3	9.9	[26]
13	70	27.9	329.2	8.49	[26]
15	50	24.2	194.4	12.4	[45]

Electrodialysis (ED)

Table 3 Electrodialysis data

C_0 (mM)	R_w (%)	ΔG_W (Wh/m^3)	SEC (Wh/m^3)	TEE (%)	Rf
86	50	109.9	1675	6.56	[46]
86	50	109.9	2141.3	5.13	[46]
86	50	109.9	2369.2	4.64	[46]
86	50	109.9	2717.7	4.04	[46]
86	50	109.9	2913.4	3.77	[46]
10	50	19.1	133.3	14.31	[47]
10	50	19	139.6	13.59	[48]
10	50	19.1	291.7	6.54	[48]
45	50	59.7	530	11.27	[42]
48	50	79	1500	5.27	[42]
403	50	132.2	3800	3.48	[49]
154	50	146.4	2780	5.27	[49]
Not Reported		482.9	1053.7	45.83	[50]
		482.9	3556.1	13.58	[50]
		248.8	643.9	38.64	[50]
		248.8	1317.1	18.89	[50]
		248.8	2443.9	10.18	[50]
		248.8	4639	5.36	[50]
		102.4	307.3	33.33	[50]
		102.4	790.2	12.96	[50]
		102.4	1536.6	6.67	[50]
		102.4	2912.2	3.52	[50]

Capacitive deionization (CDI)

Table 4 Capacitive deionization data

C_0 (mM)	C_D (mM)	R_w (%)	ΔG_W (Wh/m^3)	SEC (Wh/m^3)	TEE (%)	Type	Rf
20	9.1	50	8.65	350 - 207	2.47 - 4.17	MCDI	[51]
20	9.8	50	7.52	320	2.35	MCDI	[51]
20	12.9	50	3.57	69.3	5.15	MCDI	[51]
3.42	0.9	60	3.18	193	1.65	MCDI	[52]
40	22.3	50	11.2	745 - 535	1.50 - 2.209	MCDI	[53]
3,4	0.4	60	4.88	135	3.6	MCDI	[54]
10	6.2	50	2	177	1.13	FaCDI	[54]
3.2	1.7	67	1.41	208	0.675	CDI	[55]

3	1.8	67	0.88	107	0.825	CDI	[55]
3.5	2.4	67	0.73	74.2	0.982	CDI	[55]
2.9	2.6	67	0.074	48.8	0.152	CDI	[54]
8.7	6.8	50	0.61	50	1.23	CDI	[56]
8.7	4.4	50	0.31	2.35	0.131	CDI	[57]
8.6	2.7	50	0.62	343 - 25.7	1.80 - 2.240	MCDI	[58]
8.6	3.3	50	0.48	28.1 - 7.77	1.70 - 2.70	MCDI	[58]
8.6	3.9	50	0.37	30.8 - 6.61	1.20 - 2.230	MCDI	[58]
8.6	4.4	50	0.29	22.7 - 10.9	1.30 - 2.70	MCDI	[58]
8.6	5.3	50	0.18	25.8 - 6.95	0.7 - 2.60	MCDI	[58]
8.6	6.1	50	0.1	20.4 - 4.35	0.49 - 2.230	MCDI	[58]
10	8.6	69	0.39	11.2 - 6.98	3.50 - 5.562	CDI	[59]
10	8.8	50	0.22	16.8	1.29	CDI	[59]
20	18.4	50	0.18	8.34 - 8.817	2.12 - 2.216	CDI	[60]
5	3.5	50	0.66	61.1	1107	CDI	[56]
5	3.8	50	0.41	47.2	0.863	CDI	[56]
10	8.6	50	0.28	29.5 - 2.21	0,931 - 1.24	MCDI	[61]
10	8.5	50	0.32	67.6	0.473	FaCDI	[62]
4.3	3.5	50	0.2	47.8	0.421	i-CDI	[63]
4.3	3.9	50	0.057	45.7	1.24	i-CDI	[63]
5	4.2	50	0.177	52.8	0.335	FaCDI	[64]
5	4.3	50	0.151	24.4	0.62	CDI	[65]
5	4.74	50	0.0186	8.58	0.217	CDI	[65]
5	4.9	50	1.76E-03	0.783	0.225	CDI	[65]
10	9.3	50	0.0619	26.2	0.236	CDI	[66]
5	4.7	50	0.0248	10.1	0.246	MCDI	[67]
20	19.3	50	0.0319	35.7 - 21.2	0.089 - 0.15	CDI	[68]
20	19.6	50	0.011	24.7	0.0446	CDI	[68]
20	19.8	50	3.64E-03	8.9	0.0409	CDI	[68]
4.3	4.2	50	3.20E-03	6.77	0.0474	i-CDI	[69]
597	388	50	103.05	340	30.3	FaCDI	[70]
521	391	50	45.34	241.2	18.8	FaCDI	[71]
25	17.3	50	3.31	51.1	6.47	FaCDI	[72]
25	16.9	50	3.66	24	15.2	FaCDI	[72]
25	17.1	50	3.49	18.7	18.7	FaCDI	[72]
25	19	50	2	23.9	8.4	FaCDI	[72]
25	19.4	50	1.75	12.6	14	FaCDI	[72]
25	19.8	50	1.5	8.4	17.8	FaCDI	[72]
25	20.9	50	0.92	13.1	7.01	FaCDI	[72]
25	21.3	50	0.77	6.71	11.4	FaCDI	[72]
25	21.4	50	0.73	5.05	14.5	FaCDI	[72]
8.56	6.4	50	0.77	1.88	40.7	FaCDI	[73]
171	1.57	50	1.61E-03	0.34	0.5	FaCDI	[74]

8.54	7.58	50	0.15	33.6	0.4	FaCDI	[75]
8.54	7.55	50	0.16	65.8	0.2	FaCDI	[75]
8.54	7.3	50	0.25	92.6	0.3	FaCDI	[75]
100	96.65	50	0.15	48.4	0.31	FaCDI	[76]
13.35	12.91	50	0.02	108	0.02	FaCDI	[77]
20	18.51	50	0.15	20.8	0.72	FaCDI	[78]
20	19.5	50	0.02	15.4	0.13	FaCDI	[78]

Electrode Materials for Capacitive Deionization

In this segment, we conducted a search for electrode materials previously employed and examined in capacitive deionization, aqueous sodium ion battery, and aqueous chlorine ion battery applications.

Table 5 Electrode material data for capacitive deionization

Material	Formula	Average Voltage (V) vs Ag/AgCl sat (KCl)	Electrolyte	System	Specific capacity (mAh/g)	current density (mA/g)	Rf
1D $Na_2V_6O_{16}$, nH_2O	$Na_2V_6O_{16}$, nH_2O	-0.2585	1 M Na_2SO_4 in H_2O	3 El	123	40	[79]
$Na_4MnV(PO_4)_3$-rGO	$Na_4MnV(PO_4)_3$-rGO	0.41	1 M Na_2SO_4 in H_2O	3 El	49	1 C	[80]
Hollow $K_{0.27}MnO_2$ nanospheres	$K_{0.27}MnO_2$	0.544	2 M Na_2SO_4 in H_2O	3 El	83	200	[81]
$Na_2FeP_2O_7$	$Na_2FeP_2O_7$	-0.006	1 M Na_2SO_4 in H_2O	3 El	55	1 C	[82]
$NaTi_2(PO_4)_3$/C	$NaTi_2(PO_4)_3$/C	-0.6	1 M Na_2SO_4 in H_2O	3 El	101	500	[83]
$NaMnO_2$	$NaMnO_2$	0.5	Aqueous 2 M CH_3COONa	3 El	55	1 C	[84]
Na4Mn9O18-RGO	Na4Mn9O18-RGO	0.543	1 M Na_2SO_4 and 0.5 M $ZnSO_4$	2 El	61.7	4 C	[85]
Crossing-linked $Na_2VTi(PO_4)_3$@C	$Na_2VTi(PO_4)_3$@C	-0.6	1 M Na_2SO_4 in H_2O	3 El	62.3	0.5 C	[86]
Crossing-linked $Na_2VTi(PO_4)_3$@C	$Na_2VTi(PO_4)_3$@C	0.3	1 M Na_2SO_4 in H_2O	3 El	63	0.5 C	[87]
Bi_2O_3@C nanoflake	Bi_2O_3@C	-0.081	1 M Na_2SO_4 + 2 M NaCl	3 El	207	2000	[88]
Pristine Bi_2O_3	Bi_2O_3	-0.081	1 M Na_2SO_4 + 2 M NaCl	3 El	245	2000	[88]
$NaTi_2(PO_4)_3$	$NaTi_2(PO_4)_3$	0.55	1M NaCl in H2O	2 El	52	1000	[89]
$Na_3MnTi(PO_4)_3$	$Na_3MnTi(PO_4)_3$	0.5	1 M Na_2SO_4 in H_2O	3 El	60	0.5 C	[90]
$NaVPO_4F$	$NaVPO_4F$	0.544	5 M $NaNO_3$	3 El	54	50	[91]
$Na_{0.44}MnO_2$	$Na_{0.44}MnO_2$	0.419	1 M sodium perchlorate + 0.5 M sodium sulfate	3 El	34	121	[92]
$NaTi_2(PO_4)_3$	$NaTi_2(PO_4)_3$	-0.75	2 M Na_2SO_4 in H_2O	3 El	133	2.0 mA cm2	[93]
$Na_4Mn_9O_{18}$	$Na_4Mn_9O_{18}$	0.488	1 M Na_2SO_4 in H_2O	3 El	45	0.5	[94]
$NaTi_2(PO_4)_3$/graphene NTPG-3	NTPG-3	-0.75	1 M Na_2SO_4 in H_2O	3 El	129.3	130	[95]
$Na_7V_4(P_2O_7)_4(PO_4)$/C	$Na_7V_4(P_2O_7)_4(PO_4)$/C	0.794	1 M Na_2SO_4 in H_2O	3 El	51.2	80	[96]
Carbon-Coated $Na_{2.2}V_{1.2}Ti_{0.8}(PO_4)_3$	$Na_{2.2}V_{1.2}Ti_{0.8}(PO_4)_3$	0.325	6 M $NaClO_4$ in H_2O	3 El	61.7	1 C	[97]

$Na_{0.5}Ti_{0.5}Mn_{0.5}O_2$	$Na_{0.5}Ti_{0.5}Mn_{0.5}O_2$	0.41	6 M $NaClO_4$ in H_2O	3 El	46	30	[98]
$NaFePO_4$	$NaFePO_4$	0.03	1 M Na_2SO_4 in H_2O	3 El	70	C/10	[99]
$Na_3V_2(PO_4)_3$	$Na_3V_2(PO_4)_3$	0.4	1 M Na_2SO_4 in H_2O	3 El	94.5	1176	[100]
$Na_3V_2O_2x(PO_4)2F_{3-2x}$/MWCNT	$Na_3V_2O_2x(PO_4)2F_{3-2x}$/MWCNT	0.7	_____	3 El	46	65	[101]
$Na_4Fe_3(PO_4)_2P_2O_7$	$Na_4Fe_3(PO_4)_2P_2O_7$	0.1	1 M Na_2SO_4 in H_2O	3 El	84	129	[102]
P2-type layered $Na_{2/3}Ni_{1/4}Mn_{3/4}O_2$	$Na_{2/3}Ni_{1/4}Mn_{3/4}O_2$	0.45	1 M Na_2SO_4 in H_2O	3 El	40	0.1 C	[103]
$Na_{0.58}MnO_2$, $_{0.48}H_2O$	$Na_{0.58}MnO_2$, $_{0.48}H_2O$	0.35	1 M Na_2SO_4 in H_2O	3 El	79	1 C	[104]
$Na_{0.7}MnO_{2.05}$	$Na_{0.7}MnO_{2.05}$	0.444	1 M Na_2SO_4 in H_2O	3 El	22.1	50	[105]
$Na_2Ti_{3/2}Mn_{1/2}(PO_4)_3$ nanodots planted in a carbon matrix	$Na_2Ti_{3/2}Mn_{1/2}(PO_4)_3$	-0.5	6 M $NaClO_4$ in H_2O	3 El	78.8	0.5C	[106]
$Na_3MgTi(PO_4)3$	$Na_3MgTi(PO_4)3$	-0.45	6 M $NaClO_4$ in H_2O	3 El	54	0.2 C	[107]
C-$LiTi_2(PO_4)_3$	$LiTi_2(PO_4)_3$	-0.847	0.5 M Na_2SO_4 in H_2O	3 El	91	138	[108]
$Na_{0.66}[Mn_{0.66}Ti_{0.34}]O_2$	$Na_{0.66}[Mn_{0.66}Ti_{0.34}]O_2$	-1.3055	1 M Na_2SO_4 in H_2O	3 El	76	2 C	[109]
$FePO_4 \cdot {}_2H_2O$	$FePO_4 \cdot {}_2H_2O$	-0.2	1 M Na_2SO_4 in H_2O	3 El	80	0.5C	[110]
nanocube (m-NiHCF)	m-NiHCF	0.55	5 M ($NaClO_4$) in H_2O	3 El	70.1	100	[111]
NaCuHCF	NaCuHCF	0.5	1 M Na_2SO_4 in H_2O	3 El	71	60	[112]
$Na_2NiFe(CN)_6$	$Na_2NiFe(CN)_6$	0.45	1 M Na_2SO_4 in H_2O	3 El	65	65	[113]
Nickel hexacyanoferrate (NiHCF)	NiHCF	0.4	1 M Na_2SO_4 in H_2O	3 El	98.88	1 mA cm-2	[114]
$Na_2MnFe(CN)_6$ hexacyanoferrates	$Na_2MnFe(CN)_6$	0.75	1 M $NaClO_4$ in H_2O	2 El	116	2.0 mA cm2	[115]
$NaFe_2(CN)_6$ Prussian	$NaFe_2(CN)_6$	0.093	1 M Na_2SO_4 in H_2O	3 El	50	1C	[116]
CoCuHCF	CoCuHCF	0.348		3 El	40	1000	[117]
Prussian blue $FeFe(CN)_6$	$FeFe(CN)_6$	0.4	1 M Na_2SO_4 in H_2O	3 El	125	250	[118]
$Na_2CoFe(CN)_6$	$Na_2CoFe(CN)_6$	0.55	1 M Na_2SO_4 in H_2O	3 El	130	130	[119]
Cobalt Hexacyanoferrate (CoHCF)	CoHCF	0.6		3 El	130		[120]
$Na_{0.4}(VO)_3[Fe(CN)_6]_{2.12}H2O$	$Na_{0.4}(VO)_3[Fe(CN)_6]_{2.12}H2O$	0.8	0.5 M Na_2SO_4 + 5 M H_2SO_4	3 El	80.1	110	[121]
$Na_2CuFe(CN)_6$	$Na_2CuFe(CN)_6$	0.5			71	60	[122]
$Na_2Zn_3[Fe(CN)_6]_2$	$Na_2Zn_3[Fe(CN)_6]_2$	0.428	1 M $NaClO_4$ in H_2O	3 El	41	120	[123]
PTCDI nanofiber	PTCDI	-0.1	1 M Na_2SO_4 in H_2O	3 El	110	30	[124]
PNTCDA	PNTCDA	-0.456	1 M $NaNO_3$ in H_2O	3 El	154	1000	[125]
Polyimide	Polyimide	-0.306	5 M $NaNO_3$	3 El	165	50	[126]
(H)SNDI	(H)SNDI	-0.197		3 El	60	86	[127]
Tubular polyaniline decorated with Prussian blue nanocrystals	PA/PANI_PB	0.4	500 mg L−1 NaCl		157		[128]
Polypyrrole grafted activated carbon and MnO2 electrodes	Py/AC/MnO2	0.3	850 mg L−1 NaCl	3 EL	30.5		[129]
Polyaniline nanotubes doped	PA/AC	0.3	1 M NaCl	3 EL	80.2778		[130]

activated carbon as an anode							
Polyoxometalate-based binder free electrode	SiW12@PANI/EGC	0	1 M NaCl	3 EL	117.34		[131]
Multifunctional group sulfobutyl ether β-cyclodextrin polymer treated CNT	CNT@SBE-b-CDP	0.244	1 M NaCl	3 EL	13.533333		[132]
Radical polymer PTMA	PTMA	0.8	1 M NaCl	3 EL	111	100	[133]
BiOCl	BiOCl	-0.256	1M NaCl in H_2O	3 El	92.1	400	[134]
CoFe layered double hydroxides (CoFe−Cl-LDH) crosslinked with CNTs (CoFe−Cl-LDH/CNT)	CoFe−Cl-LDH	-0.3	1M NaCl in H_2O	3 El	190	200	[135]
$Sb_4O_5Cl_2$	$Sb_4O_5Cl_2$	-0.4	1M NaCl in H_2O	3 El	41	600	[136]
Bi@carbon	Bi@carbon	-0.206	1M NaCl in H_2O	3 El	87.9	400	[137]
Sb@rGO	Sb@rGO	-0.5	1M NaCl in H_2O	3 El	51.6	400	[138]
poly(2,2,6,6-tetramethylpiperidinyloxy-4-yl vinylether PTVE	PTVE	0.7	0.1M NaCl in H_2O	3 El	131	60 C	[139]
AgNP-10CB	AgNP-10CB	0	1M NaCl in H_2O	2 EL	175	100	[140]
AgCl-20CNT	AgCl-20CNT	0	1M NaCl in H_2O	2 EL	140	100	[140]
ZnCo–Cl layered double hydroxide	ZnCo–Cl-LDH	0	1M NaCl in H_2O	3 El	79.777778		[141]
Activated Carbon	AC	0	1M NaCl in H_2O	3 El	24.7	100	[142]

Material	Formula	Average Voltage (V) vs Ag/AgCl sat (KCl)	Electrolyte	System	Capacitance (F/g)	current density (mA/g)	Rf
Polyhedral macrotube carbon arrays	AC_Polyhedral	-0.456	NaCl	3 EL	370		[143]
Porous C from Na_2EDTA	AC_Na_2EDTA	-0.5	1 M NaCl	3 EL	140		[144]
Pani/AC	AC/PANI	0.15	0.2 M NaCl	3 EL	213		[145]
Carbon nanotubes in-situ crosslinking the activated carbon electrode	AC/CNCL	0.044	1 M NaCl	3 EL	84		[146]
PVDF derived C/CNT	AC_PVDF/CNT	0.044	1 M NaCl	3 EL	198.9		[147]
Layered double hydroxide coated activated carbon	AC@LDH	0.3	1 M NaCl	3 EL	124		[148]
Commercial activated carbon	AC	0.1	1 M NaCl	3 EL	51.8		[149]
Carbon fiber and yak hair	CF/YK	0.444	2 g L− 1 NaCl	3 EL	219.27		[150]
CF, MW-CNT, SRGO	CF/CNT	-0.456	1 M NaCl	2 EL	128.45		[151]
Sugarcane bagasse	AC_Sugarcane	-0.5	5 mM NaC	3 EL	208		[152]
Kelp	AC_Kelp	-0.456	1 M NaCl	3 EL	190		[153]
Date seeds	AC_Date seeds	-0.4	1 M NaCl	3 EL	400		[154]
Yolk-shell	AC_Yolk-shell	0.3	1 M NaCl	3 EL	268.33		[155]

Wasted coffee grounds	AC_Coffe grounds	0.144	1 M NaCl	3 EL	180.3	[156]
Xylose	AC_Xylose	0	1 M NaCl	3 EL	187.6	[157]
Coconut shell	AC_Coconut	0		3 EL	90.2	[158]
Lotus leaf	AC_Lotus leaf	0	1 M NaCl	3 EL	225	[159]
Lignocellulose	AC_Lignocellulose	0.3	1 M NaCl	3 EL	172.9	[160]
Lignin	AC_Lignin	-0.5	1 M NaCl	3 EL	68	[161]
Glucose	AC_Glucose	0	1 M NaCl	3 EL	71	[162]
Chitin derived biochar	AC_Chitin	0		3 EL	120	[163]
Carbon polyaniline	AC_tire rubber	0.5	1 M NaCl	3 EL	168.2	[164]
Bacterial-cellulose	AC_Bacterial-cellulose	0	1 M NaCl	3 EL	335.6	[165]
MOF derived carbon N doped	PC_MOF N doped	0.5	1 M NaCl	3 EL	280	[166]
Porous carbon nanosheet N, S codoped	PC_nanosheet N, S codoped	0	1 M NaCl	3 EL	350	[167]
Porous carbon from waste polystyrene N doped	PC_ waste polystyrene N doped	0.3	1 M NaCl	3 EL	327	[168]
Mesoporous carbon N doped	Mesoporous carbon N doped	0.5	1 M NaCl	3 EL	110	[169]
Microporous carbon N doped	Microporous carbon N doped	0.5	1 M NaCl	3 EL	179.2	[170]
Carbon P doped	PC_P doped	0	1 M NaCl	3 EL	160	[171]
MOF-derived Ndoped carbon tubes	CT_MOF Nd oped	0.5	1 M NaCl	3 EL	280	[172]
AC doped with MOF	AC_doped MOF	0.25	1 M NaCl	3 EL	68	[173]
Nitrogen rich mesoporous carbon derived from ZIF-8	Mesoporous carbon_N doped	0.1	1 M NaCl	3 EL	155.83	[174]
Ag-doped hollow ZIFs-derived nanoporous carbon	PC_Ag doped	0	1 M NaCl	3 EL	210	[175]
ZIF-8 derived hierarchical carbon	ANHC	0	1 M NaCl	3 EL	360.3	[176]
Nitrogenincorporated carbon polyhedrons derived from MOFs	AC_Polyhedral N doped	0.244	1 M NaCl	3 EL	100.2	[177]
N-doped rod-like porous carbon derived from dual-ligand metal–organic	PC_N doped	0.044	1 M NaCl	3 EL	277.7	[173]
Nanopatterned MOF	PC_Nanopatterned	0.044	1 M NaCl	3 EL	195.5	[178]
ZIF-8 derived porous carbon	PC_ZIF-8	0	1 M NaCl	3 EL	275.69	[173]
N,P-doped carbon–Graphene 2D heterostructure	PC/Graphene_N P doped	0	1 M NaCl	3 EL	228	[179]
MnFe2O4-rGO composite	rGo/MnFe2O4	0.15			265	[180]
Hierarchical Mn3O4 nanowires on rGO	rGo/Mn3O4 nanowires	0.4	1 M NaCl	3 EL	437	[181]
Hierarchical composite of Ndoped carbon sphere and holey	G_hydrogel N doped	0.194	1 M NaCl	3 EL	226.5	[182]

graphene hydrogel						
MnO2 nanostructures on graphene	G/MnO2	0.3		3 EL	375	[183]
Graphene/CNTs/ ZnO NPs	G/CNT/ ZnO NPs	0.4	1 M NaCl	3 EL	280	[184]
Titanium carbide nanoparticles on graphene nanoflakes	GNF/TiC	0.15	0.1 M NaCl	3 EL	443	[185]
Solar reduced graphene oxide	rGo_solar reduced	0.4	1 M NaCl	3 EL	126	[186]
Nickel hexacyanoferrate/ reduced graphene oxide	rGo/NiHCF	0.5	1 M NaCl	3 EL	271	[187]
Tungsten carbide on graphene nanoflakes	WC@GNF	0.1	1 M NaCl	3 EL	580	[188]
Hierarchically porous 3D architectural graphene	G_HP_3D	-0.1	1 M NaCl	3 EL	190	[189]
Nitrogen and phosphorusdoped three-dimensional graphene	G_3D N P doped	0			150.88	[190]
Graphene	G	0			75.18	[191]
Graphene Sponge	G_Sponge	0.3			205.2	[192]
Graphene/carbon nanotubes (CNTs) hybrid sponge	G/CNT_Sponge	0	0.1 M NaCl		203.48	[193]

References

[1] G. W. Suter, “Review papers are important and worth writing,” *Environmental Toxicology and Chemistry*, vol. 32, no. 9. pp. 1929–1930, Sep. 2013. doi: 10.1002/etc.2316.

[2] Adrian. Bejan, *Advanced engineering thermodynamics*. Wiley, 2016.

[3] R. S. Falblsh and H. Ettouney, “MSF nuclear desalination,” 2003. [Online]. Available: www.elsevier.com/locate/desal

[4] H. E1-Dessouky, I. Alatiqi, and H. Ettouney, “Process synthesis: the multi-stage flash desalination system,” 1998.

[5] A. M. K. El-Ghonemy, “Performance test of a sea water multi-stage flash distillation plant: Case study,” *Alexandria Engineering Journal*, vol. 57, no. 4, pp. 2401–2413, Dec. 2018, doi: 10.1016/j.aej.2017.08.019.

[6] R. Borsani and S. Rebagliati, “Fundamentals and costing of MSF desalination plants and comparison with other technologies,” *Desalination*, vol. 182, no. 1–3, pp. 29–37, Nov. 2005, doi: 10.1016/j.desal.2005.03.007.

[7] O. A. Kotb, “Optimum numerical approach of a MSF desalination plant to be supplied by a new specific 650 MW power plant located on the Red Sea in Egypt,” *Ain Shams Engineering Journal*, vol. 6, no. 1, pp. 257–265, Mar. 2015, doi: 10.1016/j.asej.2014.09.001.

[8] Dr. H. Ali El Saie, “Study of the operating conditions for three large MSF desalination units each of capacity 7.2/8.6 MGD (27360/32832 Ton/Day) in Abu Dhabi, UEA.,” 1980.

[9] M. A. Darwish, M. Abdel-Jawad, and G. S. Aly, “Technical and Economical Comparison Between Large Capacity Multi Stage Flash and Reverse Osmosis Desalting Plants,” 1989.

[10] H. T. El-Dessouky, H. M. Ettouney, and Y. Al-Roumi, “Multi-stage fash desalination: present and future outlook.”

[11] M. A. Darwish and A. Alsairafi, “Technical comparison between TVC/MEB and MSF,” 2004. [Online]. Available: www.elsevier.com/locate/desal

[12] H. Sayyaadi and A. Saffari, “Thermoeconomic optimization of multi effect distillation desalination systems,” *Appl Energy*, vol. 87, no. 4, pp. 1122–1133, 2010, doi: 10.1016/j.apenergy.2009.05.023.

[13] D. Zhao, J. Xue, S. Li, H. Sun, and Q. dong Zhang, “Theoretical analyses of thermal and economical aspects of multi-effect distillation desalination dealing with high-salinity wastewater,” *Desalination*, vol. 273, no. 2–3, pp. 292–298, Jun. 2011, doi: 10.1016/j.desal.2011.01.048.

[14] P. Palenzuela, A. S. Hassan, G. Zaragoza, and D. C. Alarcón-Padilla, “Steady state model for multi-effect distillation case study: Plataforma Solar de Almería MED pilot plant,” *Desalination*, vol. 337, no. 1, pp. 31–42, Mar. 2014, doi: 10.1016/j.desal.2013.12.029.

[15] P. Fiorini and E. Sciubba, “Modular simulation and thermoeconomic analysis of a multi-effect distillation desalination plant,” *Energy*, vol. 32, no. 4, pp. 459–466, 2007, doi: 10.1016/j.energy.2006.07.037.

[16] R. Deng, L. Xie, H. Lin, J. Liu, and W. Han, “Integration of thermal energy and seawater desalination,” *Energy*, vol. 35, no. 11, pp. 4368–4374, 2010, doi: 10.1016/j.energy.2009.05.025.

[17] C. Temstet, G. Canton, J. Laborid, and A. Durantd, “A large high-performance MED plant in Sicily,” 1996.

[18] K. Ansari, H. Sayyaadi, and M. Amidpour, “Thermoeconomic optimization of a hybrid pressurized water reactor (PWR) power plant coupled to a multi effect distillation desalination system with thermo-vapor compressor (MED-TVC),” *Energy*, vol. 35, no. 5, pp. 1981–1996, 2010, doi: 10.1016/j.energy.2010.01.013.

[19] M. Al-Sahali and H. Ettouney, “Developments in thermal desalination processes: Design, energy, and costing aspects,” *Desalination*, vol. 214, no. 1–3, pp. 227–240, Aug. 2007, doi: 10.1016/j.desal.2006.08.020.

[20] T. Michels, “Recent achievements of low temperature multiple effect desalination in the western areas of Abu Dhabi, UAE,” 1993.

[21] U. Fisher, A. Aviram, and A. Gendel, “ASHDOD MULTI-EFFECT LOW TEMERATURE DESALINATION LANT REORT ON YEAR OF OERATION,” 1985.

[22] S. O. Al-Habshi, “Simulation and Economic Study of the MED-TVC Units at Umm Al Nar Desalination Plant Part of the Water Resource Management Commons,” 2002. [Online]. Available: https://scholarworks.uaeu.ac.ae/all_thesesTheses.670.https://scholarworks.uaeu.ac.ae/all_theses/670

[23] A. K. Adak and P. K. Tewari, “Technical feasibility study for coupling a desalination plant to an Advanced Heavy Water Reactor,” *Desalination*, vol. 337, no. 1, pp. 76–82, Mar. 2014, doi: 10.1016/j.desal.2013.11.004.

[24] J. M. Veza, “Mechanical vapour compression desalination plants-A case study,” 1995.

[25] D. Han, W. F. He, C. Yue, and W. H. Pu, “Study on desalination of zero-emission system based on mechanical vapor compression,” *Appl Energy*, vol. 185, pp. 1490–1496, Jan. 2017, doi: 10.1016/j.apenergy.2015.12.061.

[26] X. F. Huang, J. Ling, J. C. Xu, Y. Feng, and G. M. Li, “Advanced treatment of wastewater from an iron and steel enterprise by a constructed wetland/ultrafiltration/reverse osmosis process,” *Desalination*, vol. 269, no. 1–3, pp. 41–49, Mar. 2011, doi: 10.1016/j.desal.2010.10.040.

[27] J. Shen, B. S. Richards, and A. I. Schäfer, “Renewable energy powered membrane technology: Case study of St. Dorcas borehole in Tanzania demonstrating fluoride removal

via nanofiltration/reverse osmosis," *Sep Purif Technol*, vol. 170, pp. 445–452, Oct. 2016, doi: 10.1016/j.seppur.2016.06.042.

[28] D. Sambrailo and J. Ivic, "First land-based plant for RO desalination in Croatia," 2000.

[29] M. Belkacem, S. Bakhti, and S. Aomraoui, "Groundwater treatment by reverse osmosis: Effect of brine recycling on fouling," *Desalination Water Treat*, vol. 9, no. 1–3, pp. 54–58, 2009, doi: 10.5004/dwt.2009.752.

[30] I. H. Aljundi, "Second-law analysis of a reverse osmosis plant in Jordan," *Desalination*, vol. 239, no. 1–3, pp. 207–215, 2009, doi: 10.1016/j.desal.2008.03.019.

[31] F. Majali, H. Ettouney, N. Abdel-Jabbar, and H. Qiblawey, "Design and operating characteristics of pilot scale reverse osmosis plants," *Desalination*, vol. 222, no. 1–3, pp. 441–450, Mar. 2008, doi: 10.1016/j.desal.2007.01.169.

[32] R. L. Stover, "Seawater reverse osmosis with isobaric energy recovery devices," *Desalination*, vol. 203, no. 1–3, pp. 168–175, Feb. 2007, doi: 10.1016/j.desal.2006.03.528.

[33] E. Kalimantan, V. Praptowldodo, and A. Khalik, "Studies on seawater desalination by reverse osmosis at the Badak natural gas liquefaction plant," 2000.

[34] M. Busch and W. E. Mickols, "Reducing energy consumption in seawater desalination," *Desalination*, vol. 165, no. SUPPL., pp. 299–312, Aug. 2004, doi: 10.1016/j.desal.2004.06.035.

[35] F. Reverberi and A. Gorenflo, "Three year operational experience of a spiral-wound SWRO system with a high fouling potential feed water," *Desalination*, vol. 203, no. 1–3, pp. 100–106, Feb. 2007, doi: 10.1016/j.desal.2006.05.005.

[36] M. Petry *et al.*, "The El Coloso (Chile) reverse osmosis plant," *Desalination*, vol. 203, no. 1–3, pp. 141–152, Feb. 2007, doi: 10.1016/j.desal.2006.05.007.

[37] S. A. Avlonitis, K. Kouroumbas, and N. Vlachakis, "Energy consumption and membrane replacement cost for seawater RO desalination plants Presented at the EzlropeaJl Conjerence on Desalination and the Environment: Fresh Water for All," European Desalination SocieO~, lnlernatio~tal Water Association, 2003. [Online]. Available: www.elsevier.com/locate/desal

[38] Y. Al-Wazzan, M. Safar, S. Ebrahim, N. Bumey, and A. Mesri, "Desalting of subsurface water using spiral-wound reverse osmosis (RO) system: technical and economic assessment," ELSEVIER, 2002. [Online]. Available: www.elsevier.com/locate/desal

[39] I. Muñoz and A. R. Fernández-Alba, "Reducing the environmental impacts of reverse osmosis desalination by using brackish groundwater resources," *Water Res*, vol. 42, no. 3, pp. 801–811, 2008, doi: 10.1016/j.watres.2007.08.021.

[40] D. Prats Rico and M. Chillh Arias, “A reverse osmosis potable water plant at Alicante University: first years of operation,” 2001. [Online]. Available: www.elsevier.com/bcate/desal

[41] M. A. Alghoul, P. Poovanaesvaran, K. Sopian, and M. Y. Sulaiman, “Review of brackish water reverse osmosis (BWRO) system designs,” *Renewable and Sustainable Energy Reviews*, vol. 13, no. 9. pp. 2661–2667, Dec. 2009. doi: 10.1016/j.rser.2009.03.013.

[42] K. Walha, R. Ben Amar, L. Firdaous, F. Quéméneur, and P. Jaouen, “Brackish groundwater treatment by nanofiltration, reverse osmosis and electrodialysis in Tunisia: performance and cost comparison,” *Desalination*, vol. 207, no. 1–3, pp. 95–106, Mar. 2007, doi: 10.1016/j.desal.2006.03.583.

[43] M. D. Afonsoa, J. 0 Jaberb, and M. S. Mohsenb, “Brackish groundwater treatment by reverse osmosis in Jordan,” 2004.

[44] D. Sambrailo, J. Ivić, and A. Krstulović, “Economic evaluation of the first desalination plant in Croatia,” *Desalination*, vol. 179, no. 1-3 SPEC. ISS., pp. 339–344, Jul. 2005, doi: 10.1016/j.desal.2004.11.080.

[45] M. Belkacem, S. Bekhti, and K. Bensadok, “Groundwater treatment by reverse osmosis,” *Desalination*, vol. 206, no. 1–3, pp. 100–106, Feb. 2007, doi: 10.1016/j.desal.2006.02.062.

[46] P. Malek, J. M. Ortiz, and H. M. A. Schulte-Herbrüggen, “Decentralized desalination of brackish water using an electrodialysis system directly powered by wind energy,” *Desalination*, vol. 377, pp. 54–64, Jan. 2016, doi: 10.1016/j.desal.2015.08.023.

[47] N. Kabay, Ö. Ipek, H. Kahveci, and M. Yüksel, “Effect of salt combination on separation of monovalent and divalent salts by electrodialysis,” *Desalination*, vol. 198, no. 1–3, pp. 84–91, Oct. 2006, doi: 10.1016/j.desal.2006.09.013.

[48] M. Demircioglu, N. Kabay, I. Kurucaovali, and E. Ersoz, “Demineralization by electrodialysis (ED)-separation performance and cost comparison for monovalent salts.” [Online]. Available: www.elsevier.com/locate/desal

[49] T. Chakrabarty *et al.*, “Stable ion-exchange membranes for water desalination by electrodialysis,” *Desalination*, vol. 282, pp. 2–8, Nov. 2011, doi: 10.1016/j.desal.2011.08.009.

[50] A. H. Galama, M. Saakes, H. Bruning, H. H. M. Rijnaarts, and J. W. Post, “Seawater predesalination with electrodialysis,” *Desalination*, vol. 342, pp. 61–69, Jun. 2014, doi: 10.1016/j.desal.2013.07.012.

[51] R. Zhao, P. M. Biesheuvel, and A. Van Der Wal, “Energy consumption and constant current operation in membrane capacitive deionization,” *Energy Environ Sci*, vol. 5, no. 11, pp. 9520–9527, Nov. 2012, doi: 10.1039/c2ee21737f.

[52] Y. J. Kim and J. H. Choi, “Enhanced desalination efficiency in capacitive deionization with an ion-selective membrane,” *Sep Purif Technol*, vol. 71, no. 1, pp. 70–75, Jan. 2010, doi: 10.1016/j.seppur.2009.10.026.

[53] R. Zhao, S. Porada, P. M. Biesheuvel, and A. Van der Wal, “Energy consumption in membrane capacitive deionization for different water recoveries and flow rates, and comparison with reverse osmosis,” *Desalination*, vol. 330, pp. 35–41, Dec. 2013, doi: 10.1016/j.desal.2013.08.017.

[54] J. Lee, S. Kim, C. Kim, and J. Yoon, “Hybrid capacitive deionization to enhance the desalination performance of capacitive techniques,” *Energy Environ Sci*, vol. 7, no. 11, pp. 3683–3689, Nov. 2014, doi: 10.1039/c4ee02378a.

[55] J. H. Lee, W. S. Bae, and J. H. Choi, “Electrode reactions and adsorption/desorption performance related to the applied potential in a capacitive deionization process,” *Desalination*, vol. 258, no. 1–3, pp. 159–163, Aug. 2010, doi: 10.1016/j.desal.2010.03.020.

[56] S. Porada *et al.*, “Water desalination using capacitive deionization with microporous carbon electrodes,” *ACS Appl Mater Interfaces*, vol. 4, no. 3, pp. 1194–1199, Mar. 2012, doi: 10.1021/am201683j.

[57] Joseph C. Farme, “Capacitive Deionization of NaCI and NaNO3 Solutions withCarbon Aerogel Electrodes”.

[58] P. Długołecki and A. Van Der Wal, “Energy recovery in membrane capacitive deionization,” *Environ Sci Technol*, vol. 47, no. 9, pp. 4904–4910, May 2013, doi: 10.1021/es3053202.

[59] J. Kang, T. Kim, K. Jo, and J. Yoon, “Comparison of salt adsorption capacity and energy consumption between constant current and constant voltage operation in capacitive deionization,” *Desalination*, vol. 352, pp. 52–57, Nov. 2014, doi: 10.1016/j.desal.2014.08.009.

[60] T. Kim, J. E. Dykstra, S. Porada, A. van der Wal, J. Yoon, and P. M. Biesheuvel, “Enhanced charge efficiency and reduced energy use in capacitive deionization by increasing the discharge voltage,” *J Colloid Interface Sci*, vol. 446, pp. 317–326, May 2015, doi: 10.1016/j.jcis.2014.08.041.

[61] J. Kang, T. Kim, H. Shin, J. Lee, J. I. Ha, and J. Yoon, “Direct energy recovery system for membrane capacitive deionization,” *Desalination*, vol. 398, pp. 144–150, Nov. 2016, doi: 10.1016/j.desal.2016.07.025.

[62] S. Kim, J. Lee, C. Kim, and J. Yoon, “Na2FeP2O7 as a Novel Material for Hybrid Capacitive Deionization,” *Electrochim Acta*, vol. 203, pp. 265–271, Jun. 2016, doi: 10.1016/j.electacta.2016.04.056.

[63] X. Gao, A. Omosebi, J. Landon, and K. Liu, “Enhanced Salt Removal in an Inverted Capacitive Deionization Cell Using Amine Modified Microporous Carbon Cathodes,” *Environ Sci Technol*, vol. 49, no. 18, pp. 10920–10926, Sep. 2015, doi: 10.1021/acs.est.5b02320.

[64] Y. H. Liu, H. C. Hsi, K. C. Li, and C. H. Hou, “Electrodeposited manganese dioxide/activated carbon composite as a high-performance electrode material for capacitive deionization,” *ACS Sustain Chem Eng*, vol. 4, no. 9, pp. 4762–4770, Sep. 2016, doi: 10.1021/acssuschemeng.6b00974.

[65] R. Zhao, P. M. Biesheuvel, H. Miedema, H. Bruning, and A. van der Wal, “Charge efficiency: A functional tool to probe the double-layer structure inside of porous electrodes and application in the modeling of capacitive deionization,” *Journal of Physical Chemistry Letters*, vol. 1, no. 1, pp. 205–210, Jan. 2010, doi: 10.1021/jz900154h.

[66] P. M. Biesheuvel, B. Van Limpt, and A. Van Der Wal, “Dynamic adsorption/desorption process model for capacitive deionization,” *Journal of Physical Chemistry C*, vol. 113, no. 14, pp. 5636–5640, Apr. 2009, doi: 10.1021/jp809644s.

[67] A. Omosebi, X. Gao, J. Landon, and K. Liu, “Asymmetric electrode configuration for enhanced membrane capacitive deionization,” *ACS Appl Mater Interfaces*, vol. 6, no. 15, pp. 12640–12649, Aug. 2014, doi: 10.1021/am5026209.

[68] S. Ahualli, G. R. Iglesias, M. M. Fernández, M. L. Jiménez, and Á. V. Delgado, “Use of Soft Electrodes in Capacitive Deionization of Solutions,” *Environ Sci Technol*, vol. 51, no. 9, pp. 5326–5333, May 2017, doi: 10.1021/acs.est.6b06181.

[69] X. Gao, A. Omosebi, J. Landon, and K. Liu, “Surface charge enhanced carbon electrodes for stable and efficient capacitive deionization using inverted adsorption-desorption behavior,” *Energy Environ Sci*, vol. 8, no. 3, pp. 897–909, Mar. 2015, doi: 10.1039/c4ee03172e.

[70] J. Lee, S. Kim, and J. Yoon, “Rocking Chair Desalination Battery Based on Prussian Blue Electrodes,” *ACS Omega*, vol. 2, no. 4, pp. 1653–1659, Apr. 2017, doi: 10.1021/acsomega.6b00526.

[71] M. Pasta, C. D. Wessells, Y. Cui, and F. La Mantia, “A desalination battery,” *Nano Lett*, vol. 12, no. 2, pp. 839–843, Feb. 2012, doi: 10.1021/nl203889e.

[72] T. Kim, C. A. Gorski, and B. E. Logan, “Low Energy Desalination Using Battery Electrode Deionization,” *Environ Sci Technol Lett*, vol. 4, no. 10, pp. 444–449, Oct. 2017, doi: 10.1021/acs.estlett.7b00392.

[73] S. Choi, B. Chang, S. Kim, J. Lee, J. Yoon, and J. W. Choi, “Battery Electrode Materials with Omnivalent Cation Storage for Fast and Charge-Efficient Ion Removal of Asymmetric Capacitive Deionization,” *Adv Funct Mater*, vol. 28, no. 35, Aug. 2018, doi: 10.1002/adfm.201802665.

[74] W. Shi *et al.*, "High-Performance Capacitive Deionization via Manganese Oxide-Coated, Vertically Aligned Carbon Nanotubes," *Environ Sci Technol Lett*, vol. 5, no. 11, pp. 692–700, Nov. 2018, doi: 10.1021/acs.estlett.8b00397.

[75] T. Wu *et al.*, "Highly Stable Hybrid Capacitive Deionization with a MnO2 Anode and a Positively Charged Cathode," *Environ Sci Technol Lett*, vol. 5, no. 2, pp. 98–102, Feb. 2018, doi: 10.1021/acs.estlett.7b00540.

[76] S. Hand and R. D. Cusick, "Characterizing the Impacts of Deposition Techniques on the Performance of MnO2 Cathodes for Sodium Electrosorption in Hybrid Capacitive Deionization," *Environ Sci Technol*, vol. 51, no. 20, pp. 12027–12034, Oct. 2017, doi: 10.1021/acs.est.7b03060.

[77] F. Chen, Y. Huang, L. Guo, L. Sun, Y. Wang, and H. Y. Yang, "Dual-ions electrochemical deionization: A desalination generator," *Energy Environ Sci*, vol. 10, no. 10, pp. 2081–2089, Oct. 2017, doi: 10.1039/c7ee00855d.

[78] S. Porada, A. Shrivastava, P. Bukowska, P. M. Biesheuvel, and K. C. Smith, "Nickel Hexacyanoferrate Electrodes for Continuous Cation Intercalation Desalination of Brackish Water," *Electrochim Acta*, vol. 255, pp. 369–378, Nov. 2017, doi: 10.1016/j.electacta.2017.09.137.

[79] C. Deng, S. Zhang, Z. Dong, and Y. Shang, "1D nanostructured sodium vanadium oxide as a novel anode material for aqueous sodium ion batteries," *Nano Energy*, vol. 4, pp. 49–55, Mar. 2014, doi: 10.1016/j.nanoen.2013.12.014.

[80] P. Ramesh Kumar *et al.*, "Na4MnV(PO4)3-rGO as Advanced cathode for aqueous and non-aqueous sodium ion batteries," *J Power Sources*, vol. 429, pp. 149–155, Jul. 2019, doi: 10.1016/j.jpowsour.2019.04.080.

[81] Y. Liu, Y. Qiao, X. Lou, X. Zhang, W. Zhang, and Y. Huang, "Hollow K0.27MnO2 Nanospheres as Cathode for High-Performance Aqueous Sodium Ion Batteries," *ACS Appl Mater Interfaces*, vol. 8, no. 23, pp. 14564–14571, Jun. 2016, doi: 10.1021/acsami.6b03089.

[82] Y. H. Jung, H. Lim, and D. K. Kim, "Electrochemical characterizations of Na 2 FeP 2 O 7 as an aqueous sodium-ion battery electrode," 2013.

[83] X. Wu, Y. Cao, X. Ai, J. Qian, and H. Yang, "A low-cost and environmentally benign aqueous rechargeable sodium-ion battery based on NaTi2(PO4)3-Na 2NiFe(CN)6 intercalation chemistry," *Electrochem commun*, vol. 31, pp. 145–148, Jun. 2013, doi: 10.1016/j.elecom.2013.03.013.

[84] Z. Hou, X. Li, J. Liang, Y. Zhu, and Y. Qian, "An aqueous rechargeable sodium ion battery based on a NaMnO2-NaTi2(PO4)3 hybrid system for stationary energy storage," *J Mater Chem A Mater*, vol. 3, no. 4, pp. 1400–1404, Jan. 2015, doi: 10.1039/c4ta06018k.

[85] F. Yin, Z. Liu, Y. Zhao, Y. Feng, and Y. Zhang, “Electrochemical properties of an Na4Mn9O18-reduced graphene oxide composite synthesized via spray drying for an aqueous sodium-ion battery,” *Nanomaterials*, vol. 7, no. 9, Sep. 2017, doi: 10.3390/nano7090253.

[86] J. Dong, G. Zhang, X. Wang, S. Zhang, and C. Deng, “Cross-linked Na2VTi(PO4)3@C hierarchical nanofibers as high-performance bi-functional electrodes for symmetric aqueous rechargeable sodium batteries,” *J Mater Chem A Mater*, vol. 5, no. 35, pp. 18725–18736, 2017, doi: 10.1039/c7ta05361d.

[87] J. Dong, G. Zhang, X. Wang, S. Zhang, and C. Deng, “Cross-linked Na2VTi(PO4)3@C hierarchical nanofibers as high-performance bi-functional electrodes for symmetric aqueous rechargeable sodium batteries,” *J Mater Chem A Mater*, vol. 5, no. 35, pp. 18725–18736, 2017, doi: 10.1039/c7ta05361d.

[88] Z. Zhao, Y. Ye, W. Zhu, L. Xiao, B. Deng, and J. Liu, “Bismuth oxide nanoflake@carbon film: A free-standing battery-type electrode for aqueous sodium ion hybrid supercapacitors,” *Chinese Chemical Letters*, vol. 29, no. 4, pp. 629–632, Apr. 2018, doi: 10.1016/j.cclet.2018.01.011.

[89] F. Chen, Y. Huang, D. Kong, M. Ding, S. Huang, and H. Y. Yang, “NaTi2(PO4)3-Ag electrodes based desalination battery and energy recovery,” *FlatChem*, vol. 8, pp. 9–16, Mar. 2018, doi: 10.1016/j.flatc.2018.02.001.

[90] H. Gao and J. B. Goodenough, “ An Aqueous Symmetric Sodium-Ion Battery with NASICON-Structured Na 3 MnTi(PO 4) 3 ,” *Angewandte Chemie*, vol. 128, no. 41, pp. 12960–12964, Oct. 2016, doi: 10.1002/ange.201606508.

[91] H. Qin, Z. P. Song, H. Zhan, and Y. H. Zhou, “Aqueous rechargeable alkali-ion batteries with polyimide anode,” *J Power Sources*, vol. 249, pp. 367–372, 2014, doi: 10.1016/j.jpowsour.2013.10.091.

[92] D. J. Kim *et al.*, “Diffusion behavior of sodium ions in Na0.44MnO2 in aqueous and non-aqueous electrolytes,” *J Power Sources*, vol. 244, pp. 758–763, 2013, doi: 10.1016/j.jpowsour.2013.02.090.

[93] S. Il Park, I. Gocheva, S. Okada, and J. Yamaki, “Electrochemical Properties of NaTi2(PO4)3 Anode for Rechargeable Aqueous Sodium-Ion Batteries,” *J Electrochem Soc*, vol. 158, no. 10, p. A1067, 2011, doi: 10.1149/1.3611434.

[94] J. F. Whitacre, A. Tevar, and S. Sharma, “Na4Mn9O18 as a positive electrode material for an aqueous electrolyte sodium-ion energy storage device,” *Electrochem commun*, vol. 12, no. 3, pp. 463–466, Mar. 2010, doi: 10.1016/j.elecom.2010.01.020.

[95] X. Li *et al.*, “ Graphene-Supported NaTi 2 (PO 4) 3 as a High Rate Anode Material for Aqueous Sodium Ion Batteries ,” *J Electrochem Soc*, vol. 161, no. 6, pp. A1181–A1187, 2014, doi: 10.1149/2.0081409jes.

[96] C. Deng, S. Zhang, and Y. Wu, “Hydrothermal-assisted synthesis of the Na7V4(P2O7)4(PO4)/C nanorod and its fast sodium intercalation chemistry in aqueous rechargeable sodium batteries,” *Nanoscale*, vol. 7, no. 2, pp. 487–491, Jan. 2015, doi: 10.1039/c4nr05175k.

[97] P. Lei, Y. Wang, F. Zhang, X. Wan, and X. Xiang, “Carbon-Coated Na2.2V1.2Ti0.8(PO4)3 Cathode with Excellent Cycling Performance for Aqueous Sodium-Ion Batteries,” *ChemElectroChem*, vol. 5, no. 17, pp. 2482–2487, Sep. 2018, doi: 10.1002/celc.201800379.

[98] F. Zhang, W. Li, X. Xiang, and M. Sun, “Highly stable Na-storage performance of Na0.5Mn0.5Ti0.5O2 microrods as cathode for aqueous sodium-ion batteries,” *Journal of Electroanalytical Chemistry*, vol. 802, pp. 22–26, Oct. 2017, doi: 10.1016/j.jelechem.2017.08.042.

[99] A. J. Fernández-Ropero, D. Saurel, B. Acebedo, T. Rojo, and M. Casas-Cabanas, “Electrochemical characterization of NaFePO4 as positive electrode in aqueous sodium-ion batteries,” *J Power Sources*, vol. 291, pp. 40–45, May 2015, doi: 10.1016/j.jpowsour.2015.05.006.

[100] L. Zhang, T. Huang, and A. Yu, “Carbon-coated Na3V2(PO4)3 nanocomposite as a novel high rate cathode material for aqueous sodium ion batteries,” *J Alloys Compd*, vol. 646, pp. 522–527, Jun. 2015, doi: 10.1016/j.jallcom.2015.05.126.

[101] P. R. Kumar, Y. H. Jung, C. H. Lim, and D. K. Kim, “Na3V2O2x(PO4)2F3-2x: A stable and high-voltage cathode material for aqueous sodium-ion batteries with high energy density,” *J Mater Chem A Mater*, vol. 3, no. 12, pp. 6271–6275, Mar. 2015, doi: 10.1039/c5ta00980d.

[102] A. J. Fernández-Ropero, M. Zarrabeitia, M. Reynaud, T. Rojo, and M. Casas-Cabanas, “Toward Safe and Sustainable Batteries: Na4Fe3(PO4)2P2O7 as a Low-Cost Cathode for Rechargeable Aqueous Na-Ion Batteries,” *Journal of Physical Chemistry C*, vol. 122, no. 1, pp. 133–142, Jan. 2018, doi: 10.1021/acs.jpcc.7b09803.

[103] F. Yu *et al.*, “Electrochemical characterization of P2-type layered Na2/3Ni1/4Mn3/4O2 cathode in aqueous hybrid sodium/lithium ion electrolyte,” *Ceram Int*, vol. 43, no. 13, pp. 9960–9967, 2017, doi: 10.1016/j.ceramint.2017.05.007.

[104] F. Zhang, W. Li, X. Xiang, and M. Sun, “Highly stable Na-storage performance of Na0.5Mn0.5Ti0.5O2 microrods as cathode for aqueous sodium-ion batteries,” *Journal of Electroanalytical Chemistry*, vol. 802, pp. 22–26, Oct. 2017, doi: 10.1016/j.jelechem.2017.08.042.

[105] F. Gu *et al.*, “Studies on micron-sized Na0.7MnO2.05 with excellent cycling performance as a cathode material for aqueous rechargeable sodium-ion batteries,” *Appl Phys A Mater Sci Process*, vol. 126, no. 8, Aug. 2020, doi: 10.1007/s00339-020-03799-6.

[106] P. Lei, K. Liu, X. Wan, D. Luo, and X. Xiang, “Ultrafast Na intercalation chemistry of Na2Ti3/2Mn1/2(PO4)3 nanodots planted in a carbon matrix as a low cost anode for aqueous sodium-ion batteries,” *Chemical Communications*, vol. 55, no. 4, pp. 509–512, 2019, doi: 10.1039/c8cc07668e.

[107] F. Zhang, W. Li, X. Xiang, and M. Sun, “Nanocrystal-Assembled Porous Na3MgTi(PO4)3 Aggregates as Highly Stable Anode for Aqueous Sodium-Ion Batteries,” *Chemistry - A European Journal*, vol. 23, no. 52, pp. 12944–12948, Sep. 2017, doi: 10.1002/chem.201703044.

[108] N. Arun, V. Aravindan, W. C. Ling, and S. Madhavi, “Carbon coated LiTi2(PO4)3 as new insertion anode for aqueous Na-ion batteries,” *Journal of Alloys and Compounds*, vol. 603. Elsevier Ltd, pp. 48–51, Aug. 05, 2014. doi: 10.1016/j.jallcom.2014.03.059.

[109] Y. Wang *et al.*, “A Novel High Capacity Positive Electrode Material with Tunnel-Type Structure for Aqueous Sodium-Ion Batteries,” *Adv Energy Mater*, vol. 5, no. 22, Nov. 2015, doi: 10.1002/aenm.201501005.

[110] Y. Wang *et al.*, “Ultra-low cost and highly stable hydrated FePO4 anodes for aqueous sodium-ion battery,” *J Power Sources*, vol. 374, pp. 211–216, Jan. 2018, doi: 10.1016/j.jpowsour.2017.10.088.

[111] L. Shen, Y. Jiang, Y. Liu, J. Ma, T. Sun, and N. Zhu, “High-stability monoclinic nickel hexacyanoferrate cathode materials for ultrafast aqueous sodium ion battery,” *Chemical Engineering Journal*, vol. 388, May 2020, doi: 10.1016/j.cej.2020.124228.

[112] X. Y. Wu *et al.*, “Energetic aqueous rechargeable sodium-ion battery based on Na 2CuFe(CN)6-NaTi2(PO4)3 intercalation chemistry,” *ChemSusChem*, vol. 7, no. 2, pp. 407–411, Feb. 2014, doi: 10.1002/cssc.201301036.

[113] K. Krishnamoorthy, P. Pazhamalai, S. Sahoo, J. H. Lim, K. H. Choi, and S. J. Kim, “A High-Energy Aqueous Sodium-Ion Capacitor with Nickel Hexacyanoferrate and Graphene Electrodes,” *ChemElectroChem*, vol. 4, no. 12, pp. 3302–3308, Dec. 2017, doi: 10.1002/celc.201700690.

[114] X. Wu, Y. Cao, X. Ai, J. Qian, and H. Yang, “A low-cost and environmentally benign aqueous rechargeable sodium-ion battery based on NaTi2(PO4)3-Na 2NiFe(CN)6 intercalation chemistry,” *Electrochem commun*, vol. 31, pp. 145–148, Jun. 2013, doi: 10.1016/j.elecom.2013.03.013.

[115] K. Nakamoto, R. Sakamoto, M. Ito, A. Kitajou, and S. Okada, “Effect of concentrated electrolyte on aqueous sodium-ion battery with sodium manganese hexacyanoferrate cathode,” *Electrochemistry*, vol. 85, no. 4, pp. 179–185, 2017, doi: 10.5796/electrochemistry.85.179.

[116] A. J. Fernández-Ropero, M. J. Piernas-Muñoz, E. Castillo-Martínez, T. Rojo, and M. Casas-Cabanas, “Electrochemical characterization of NaFe2(CN)6 Prussian Blue as

positive electrode for aqueous sodium-ion batteries," *Electrochim Acta*, vol. 210, pp. 352–357, Aug. 2016, doi: 10.1016/j.electacta.2016.05.176.

[117] D. J. Kim *et al.*, "An aqueous sodium ion hybrid battery incorporating an organic compound and a prussian blue derivative," *Adv Energy Mater*, vol. 4, no. 12, Aug. 2014, doi: 10.1002/aenm.201400133.

[118] X. Wu *et al.*, "Low-defect Prussian blue nanocubes as high capacity and long life cathodes for aqueous Na-ion batteries," *Nano Energy*, vol. 13, pp. 117–123, Apr. 2015, doi: 10.1016/j.nanoen.2015.02.006.

[119] X. Wu *et al.*, "Vacancy-Free Prussian Blue Nanocrystals with High Capacity and Superior Cyclability for Aqueous Sodium-Ion Batteries," *ChemNanoMat*, vol. 1, no. 3, pp. 188–193, Jul. 2015, doi: 10.1002/cnma.201500021.

[120] S. H. M. H. Tehrani, S. A. Seyedsadjadi, and A. Ghaffarinejad, "Application of electrodeposited cobalt hexacyanoferrate film to extract energy from water salinity gradients," *RSC Adv*, vol. 5, no. 38, pp. 30032–30037, 2015, doi: 10.1039/c5ra03909f.

[121] J. H. Lee, G. Ali, D. H. Kim, and K. Y. Chung, "Metal-Organic Framework Cathodes Based on a Vanadium Hexacyanoferrate Prussian Blue Analogue for High-Performance Aqueous Rechargeable Batteries," *Adv Energy Mater*, vol. 7, no. 2, Jan. 2017, doi: 10.1002/aenm.201601491.

[122] X. Y. Wu *et al.*, "Energetic aqueous rechargeable sodium-ion battery based on Na 2CuFe(CN)6-NaTi2(PO4)3 intercalation chemistry," *ChemSusChem*, vol. 7, no. 2, pp. 407–411, Feb. 2014, doi: 10.1002/cssc.201301036.

[123] M. Shao *et al.*, "A High-Voltage and Cycle Stable Aqueous Rechargeable Na-Ion Battery Based on Na2Zn3[Fe(CN)6]2-NaTi2(PO4)3 Intercalation Chemistry," *ACS Appl Energy Mater*, vol. 2, no. 8, pp. 5809–5815, Aug. 2019, doi: 10.1021/acsaem.9b00935.

[124] L. Yang *et al.*, "Flexible and additive-free organic electrodes for aqueous sodium ion batteries," *J Mater Chem A Mater*, vol. 8, no. 43, pp. 22791–22801, Nov. 2020, doi: 10.1039/d0ta07267b.

[125] X. Dong, L. Chen, J. Liu, S. Haller, Y. Wang, and Y. Xia, "Environmentally-friendly aqueous Li (or Na)-ion battery with fast electrode kinetics and super-long life," *Sci Adv*, vol. 2, no. 1, Jan. 2016, doi: 10.1126/sciadv.1501038.

[126] H. Qin, Z. P. Song, H. Zhan, and Y. H. Zhou, "Aqueous rechargeable alkali-ion batteries with polyimide anode," *J Power Sources*, vol. 249, pp. 367–372, 2014, doi: 10.1016/j.jpowsour.2013.10.091.

[127] D. J. Kim *et al.*, "An aqueous sodium ion hybrid battery incorporating an organic compound and a prussian blue derivative," *Adv Energy Mater*, vol. 4, no. 12, Aug. 2014, doi: 10.1002/aenm.201400133.

[128] W. Shi *et al.*, "Enabling Superior Sodium Capture for Efficient Water Desalination by a Tubular Polyaniline Decorated with Prussian Blue Nanocrystals," *Advanced Materials*, vol. 32, no. 33, Aug. 2020, doi: 10.1002/adma.201907404.

[129] G. Tan, S. Lu, N. Xu, D. Gao, and X. Zhu, "Pseudocapacitive Behaviors of Polypyrrole Grafted Activated Carbon and MnO2 Electrodes to Enable Fast and Efficient Membrane-Free Capacitive Deionization," *Environ Sci Technol*, vol. 54, no. 9, pp. 5843–5852, May 2020, doi: 10.1021/acs.est.9b07182.

[130] P. Nie, J. Yan, G. Zhu, and J. Liu, "Inverted hybrid-capacitive deionization with polyaniline nanotubes doped activated carbon as an anode," *Electrochim Acta*, vol. 339, Apr. 2020, doi: 10.1016/j.electacta.2020.135920.

[131] H. Liu, J. Zhang, X. Xu, and Q. Wang, "A Polyoxometalate-Based Binder-Free Capacitive Deionization Electrode for Highly Efficient Sea Water Desalination," *Chemistry - A European Journal*, vol. 26, no. 19, pp. 4403–4409, Apr. 2020, doi: 10.1002/chem.201905606.

[132] D. Ma, Y. Wang, Y. Cai, S. Xu, and J. Wang, "Multifunctional group sulfobutyl ether β-cyclodextrin polymer treated CNT as the cathode for enhanced performance in asymmetric capacitive deionization," *Electrochim Acta*, vol. 313, pp. 321–330, Aug. 2019, doi: 10.1016/j.electacta.2019.05.041.

[133] Y. Li, Z. Ding, J. Li, K. Wang, T. Lu, and L. Pan, "Novel membrane-free hybrid capacitive deionization with a radical polymer anode for stable desalination," *Desalination*, vol. 481, May 2020, doi: 10.1016/j.desal.2020.114379.

[134] F. Chen, Z. Y. Leong, and H. Y. Yang, "An aqueous rechargeable chloride ion battery," *Energy Storage Mater*, vol. 7, pp. 189–194, Apr. 2017, doi: 10.1016/j.ensm.2017.02.001.

[135] Z. Wu, Y. Wu, Q. Yuan, J. Zhang, Y. Dou, and J. Han, "Aqueous Chloride-Ion Battery within a Neutral Electrolyte Based on a CoFe-Cl Layered Double Hydroxide Anode," *ACS Appl Mater Interfaces*, vol. 15, no. 32, pp. 38540–38549, Aug. 2023, doi: 10.1021/acsami.3c09706.

[136] X. Hu *et al.*, "Electrochemical Performance of Sb 4 O 5 Cl 2 as a New Anode Material in Aqueous Chloride-Ion Battery," *ACS Appl Mater Interfaces*, vol. 11, no. 9, pp. 9144–9148, Mar. 2019, doi: 10.1021/acsami.8b21652.

[137] Z. Zhang *et al.*, "The composite electrode of Bi@carbon-texture derived from metal-organic frameworks for aqueous chloride ion battery," *Ionics (Kiel)*, vol. 26, no. 5, pp. 2395–2403, May 2020, doi: 10.1007/s11581-019-03389-4.

[138] Q. Zhang *et al.*, "Sb nanoparticle decorated rGO as a new anode material in aqueous chloride ion batteries," *Nanoscale*, vol. 12, no. 23, pp. 12268–12274, Jun. 2020, doi: 10.1039/d0nr00862a.

[139] Y. Li, Z. Ding, J. Li, K. Wang, T. Lu, and L. Pan, “Novel membrane-free hybrid capacitive deionization with a radical polymer anode for stable desalination,” *Desalination*, vol. 481, May 2020, doi: 10.1016/j.desal.2020.114379.

[140] P. Srimuk, S. Husmann, and V. Presser, “Low voltage operation of a silver/silver chloride battery with high desalination capacity in seawater,” *RSC Adv*, vol. 9, no. 26, pp. 14849–14858, 2019, doi: 10.1039/c9ra02570g.

[141] Z. Zhang and H. Li, “Promoting the uptake of chloride ions by ZnCo-Cl layered double hydroxide electrodes for enhanced capacitive deionization,” *Environ Sci Nano*, vol. 8, no. 7, pp. 1886–1895, Jul. 2021, doi: 10.1039/d1en00350j.

[142] K. Koshika, N. Sano, K. Oyaizu, and H. Nishide, “An ultrafast chargeable polymer electrode based on the combination of nitroxide radical and aqueous electrolyte,” *Chemical Communications*, no. 7, pp. 836–838, 2009, doi: 10.1039/b818087c.

[143] X. Ma, Q. Wu, W. A. Wang, S. Lu, Y. Xiang, and D. Aurbach, “Mass-producible polyhedral macrotube carbon arrays with multi-hole cross-section profiles: superb 3D tertiary porous electrode materials for supercapacitors and capacitive deionization cells,” *J Mater Chem A Mater*, vol. 8, no. 32, pp. 16312–16322, Aug. 2020, doi: 10.1039/d0ta00682c.

[144] G. Tan, Q. Liu, X. Li, Y. Liu, and D. Xiao, “Porous carbon material prepared from Na2EDTA and its performance in capacitive deionization process,” *Appl Surf Sci*, vol. 496, Dec. 2019, doi: 10.1016/j.apsusc.2019.07.268.

[145] R. L. Zornitta *et al.*, “High-performance activated carbon from polyaniline for capacitive deionization,” *Carbon N Y*, vol. 123, pp. 318–333, Oct. 2017, doi: 10.1016/j.carbon.2017.07.071.

[146] J. Xie, J. Ma, L. Wu, M. Xu, W. Ni, and Y. M. Yan, “Carbon nanotubes in-situ cross-linking the activated carbon electrode for high-performance capacitive deionization,” *Sep Purif Technol*, vol. 239, May 2020, doi: 10.1016/j.seppur.2020.116593.

[147] Y. Li, J. Qi, W. Zhang, M. Zhang, and J. Li, “Fabrication of polyvinylidene fluoride-derived porous carbon heterostructure with inserted carbon nanotube via phase-inversion coupled with annealing for capacitive deionization application,” *J Colloid Interface Sci*, vol. 554, pp. 353–361, Oct. 2019, doi: 10.1016/j.jcis.2019.06.094.

[148] J. Lee, S. Kim, N. Kim, C. Kim, and J. Yoon, “Enhancing the desalination performance of capacitive deionization using a layered double hydroxide coated activated carbon electrode,” *Applied Sciences (Switzerland)*, vol. 10, no. 1, Jan. 2020, doi: 10.3390/app10010403.

[149] N. L. Liu, S. H. Sun, and C. H. Hou, “Studying the electrosorption performance of activated carbon electrodes in batch-mode and single-pass capacitive deionization,” *Sep Purif Technol*, vol. 215, pp. 403–409, May 2019, doi: 10.1016/j.seppur.2019.01.029.

[150] L. Liu, C. Zhao, F. Zheng, D. Deng, M. A. Anderson, and Y. Wang, "Three-dimensional electrode design with conductive fibers and ordered macropores for enhanced capacitive deionization performance," *Desalination*, vol. 498, Jan. 2021, doi: 10.1016/j.desal.2020.114794.

[151] D. J. Ahirrao and N. Jha, "Comparative study on the electrosorption properties of carbon fabric, functionalized multiwall carbon nanotubes and solar reduced graphene oxide for flow through electrode based desalination studies," *Carbon N Y*, vol. 152, pp. 837–850, Nov. 2019, doi: 10.1016/j.carbon.2019.06.078.

[152] Y. H. Tang, S. H. Liu, and D. C. W. Tsang, "Microwave-assisted production of CO2-activated biochar from sugarcane bagasse for electrochemical desalination," *J Hazard Mater*, vol. 383, Feb. 2020, doi: 10.1016/j.jhazmat.2019.121192.

[153] N. Sun *et al.*, "Hierarchical Porous Carbon Materials Derived from Kelp for Superior Capacitive Applications," *ACS Sustain Chem Eng*, vol. 7, no. 9, pp. 8735–8743, May 2019, doi: 10.1021/acssuschemeng.9b00635.

[154] A. Hai, G. Bharath, K. R. Babu, H. Taher, M. Naushad, and F. Banat, "Date seeds biomass-derived activated carbon for efficient removal of NaCl from saline solution," *Process Safety and Environmental Protection*, vol. 129, pp. 103–111, Sep. 2019, doi: 10.1016/j.psep.2019.06.024.

[155] X. Wei, X. Li, C. Lv, X. Mo, and K. Li, "Hierarchically yolk-shell porous carbon sphere as an electrode material for high-performance capacitive deionization," *Electrochim Acta*, vol. 354, Sep. 2020, doi: 10.1016/j.electacta.2020.136590.

[156] M. Qian, X. Y. Xuan, L. K. Pan, and S. Q. Gong, "Porous carbon electrodes from activated wasted coffee grounds for capacitive deionization," *Ionics (Kiel)*, vol. 25, no. 7, pp. 3443–3452, Jul. 2019, doi: 10.1007/s11581-019-02887-9.

[157] T. Lu *et al.*, "Highly efficient water desalination by capacitive deionization on biomass-derived porous carbon nanoflakes," *Sep Purif Technol*, vol. 256, Feb. 2021, doi: 10.1016/j.seppur.2020.117771.

[158] T. T. Nguyen *et al.*, "Enhanced capacitive deionization performance of activated carbon derived from coconut shell electrodes with low content carbon nanotubes–graphene synergistic hybrid additive," *Mater Lett*, vol. 292, Jun. 2021, doi: 10.1016/j.matlet.2021.129652.

[159] G. Liu, L. Qiu, H. Deng, J. Wang, L. Yao, and L. Deng, "Ultrahigh surface area carbon nanosheets derived from lotus leaf with super capacities for capacitive deionization and dye adsorption," *Appl Surf Sci*, vol. 524, Sep. 2020, doi: 10.1016/j.apsusc.2020.146485.

[160] T. Lu *et al.*, "High-performance capacitive deionization by lignocellulose-derived eco-friendly porous carbon materials," *Bull Chem Soc Jpn*, vol. 93, no. 8, pp. 1014–1019, Aug. 2020, doi: 10.1246/bcsj.20200055.

[161] S. Chaleawlert-Umpon and N. Pimpha, “Sustainable lignin-derived hierarchically porous carbon for capacitive deionization applications,” *New Journal of Chemistry*, vol. 44, no. 28, pp. 12058–12067, Jul. 2020, doi: 10.1039/d0nj02424d.

[162] S. K. Mohamed, M. Abuelhamd, N. K. Allam, A. Shahat, M. Ramadan, and H. M. A. Hassan, “Eco-friendly facile synthesis of glucose–derived microporous carbon spheres electrodes with enhanced performance for water capacitive deionization,” *Desalination*, vol. 477, Mar. 2020, doi: 10.1016/j.desal.2019.114278.

[163] P. Li, T. Feng, Z. Song, Y. Tan, and W. Luo, “Chitin derived biochar for efficient capacitive deionization performance,” *RSC Adv*, vol. 10, no. 50, pp. 30077–30086, Aug. 2020, doi: 10.1039/d0ra05554a.

[164] S. F. Evans *et al.*, “Carbon polyaniline capacitive deionization electrodes with stable cycle life,” *Desalination*, vol. 464, pp. 25–32, Aug. 2019, doi: 10.1016/j.desal.2019.04.002.

[165] Y. Li *et al.*, “Phosphorus-doped 3D carbon nanofiber aerogels derived from bacterial-cellulose for highly-efficient capacitive deionization,” *Carbon N Y*, vol. 130, pp. 377–383, Apr. 2018, doi: 10.1016/j.carbon.2018.01.035.

[166] X. Xu *et al.*, “Ultrahigh capacitive deionization performance by 3D interconnected MOF-derived nitrogen-doped carbon tubes,” *Chemical Engineering Journal*, vol. 390, Jun. 2020, doi: 10.1016/j.cej.2020.124493.

[167] X. Min, X. Hu, X. Li, H. Wang, and W. Yang, “Synergistic effect of nitrogen, sulfur-codoping on porous carbon nanosheets as highly efficient electrodes for capacitive deionization,” *J Colloid Interface Sci*, vol. 550, pp. 147–158, Aug. 2019, doi: 10.1016/j.jcis.2019.04.082.

[168] N. Deka, J. Barman, S. Kasthuri, V. Nutalapati, and G. K. Dutta, “Transforming waste polystyrene foam into N-doped porous carbon for capacitive energy storage and deionization applications,” *Appl Surf Sci*, vol. 511, May 2020, doi: 10.1016/j.apsusc.2020.145576.

[169] S. Tian, J. Wu, X. Zhang, K. (Ken) Ostrikov, and Z. Zhang, “Capacitive deionization with nitrogen-doped highly ordered mesoporous carbon electrodes,” *Chemical Engineering Journal*, vol. 380, Jan. 2020, doi: 10.1016/j.cej.2019.122514.

[170] D. Li, X. an Ning, Y. Huang, and S. Li, “Nitrogen-rich microporous carbon materials for high-performance membrane capacitive deionization,” *Electrochim Acta*, vol. 312, pp. 251–262, Jul. 2019, doi: 10.1016/j.electacta.2019.04.172.

[171] H. Wang *et al.*, “Enhanced chloride removal of phosphorus doping in carbon material for capacitive deionization: Experimental measurement and theoretical calculation,” *Science of the Total Environment*, vol. 720, Jun. 2020, doi: 10.1016/j.scitotenv.2020.137637.

[172] J. Zhang, T. Yan, J. Fang, J. Shen, L. Shi, and D. Zhang, “Enhanced capacitive deionization of saline water using N-doped rod-like porous carbon derived from dual-

ligand metal-organic frameworks," *Environ Sci Nano*, vol. 7, no. 3, pp. 926–937, Mar. 2020, doi: 10.1039/c9en01216h.

[173] J. Zhang, T. Yan, J. Fang, J. Shen, L. Shi, and D. Zhang, "Enhanced capacitive deionization of saline water using N-doped rod-like porous carbon derived from dual-ligand metal-organic frameworks," *Environ Sci Nano*, vol. 7, no. 3, pp. 926–937, Mar. 2020, doi: 10.1039/c9en01216h.

[174] W. Zhang *et al.*, "Core-shell hybrid zeolitic imidazolate framework-derived hierarchical carbon for capacitive deionization," *J Mater Chem A Mater*, vol. 8, no. 29, pp. 14653–14660, Aug. 2020, doi: 10.1039/d0ta05709f.

[175] W. Zhang *et al.*, "Core-shell hybrid zeolitic imidazolate framework-derived hierarchical carbon for capacitive deionization," *J Mater Chem A Mater*, vol. 8, no. 29, pp. 14653–14660, Aug. 2020, doi: 10.1039/d0ta05709f.

[176] Y. Zhao *et al.*, "Nitrogen-rich mesoporous carbons derived from zeolitic imidazolate framework-8 for efficient capacitive deionization," *Electrochim Acta*, vol. 321, Oct. 2019, doi: 10.1016/j.electacta.2019.134665.

[177] J. Kim, J. Kim, J. H. Kim, and H. S. Park, "Hierarchically open-porous nitrogen-incorporated carbon polyhedrons derived from metal-organic frameworks for improved CDI performance," *Chemical Engineering Journal*, vol. 382, Feb. 2020, doi: 10.1016/j.cej.2019.122996.

[178] X. Xu *et al.*, "Ultrahigh capacitive deionization performance by 3D interconnected MOF-derived nitrogen-doped carbon tubes," *Chemical Engineering Journal*, vol. 390, Jun. 2020, doi: 10.1016/j.cej.2020.124493.

[179] J. Guo *et al.*, "Graphene-carbon 2D heterostructures with hierarchically-porous P,N-doped layered architecture for capacitive deionization," *Chem Sci*, vol. 12, no. 30, pp. 10334–10340, Aug. 2021, doi: 10.1039/d1sc00915j.

[180] H. Younes and L. Zou, "Asymmetric configuration of pseudocapacitive composite and rGO electrodes for enhanced capacitive deionization," *Environ Sci (Camb)*, vol. 6, no. 2, pp. 392–403, Feb. 2020, doi: 10.1039/c9ew01033e.

[181] G. Bharath *et al.*, "Synthesis of hierarchical Mn3O4 nanowires on reduced graphene oxide nanoarchitecture as effective pseudocapacitive electrodes for capacitive desalination application," *Electrochim Acta*, vol. 337, Mar. 2020, doi: 10.1016/j.electacta.2020.135668.

[182] M. Mi, X. Liu, W. Kong, Y. Ge, W. Dang, and J. Hu, "Hierarchical composite of N-doped carbon sphere and holey graphene hydrogel for high-performance capacitive deionization," *Desalination*, vol. 464, pp. 18–24, Aug. 2019, doi: 10.1016/j.desal.2019.04.014.

[183] M. A. Jaoude *et al.*, "Morphology-dependent electrochemical performance of MnO2 nanostructures on graphene towards efficient capacitive deionization," *Electrochim Acta*, vol. 330, Jan. 2020, doi: 10.1016/j.electacta.2019.135202.

[184] N. Arora, F. Banat, G. Bharath, and E. Alhseinat, “Capacitive deionization of NaCl from saline solution using graphene/CNTs/ZnO NPs based electrodes,” *J Phys D Appl Phys*, vol. 52, no. 45, Aug. 2019, doi: 10.1088/1361-6463/ab3967.

[185] A. Yousef, R. M. Abdel Hameed, S. F. Shaikh, A. Abutaleb, M. M. El-Halwany, and A. M. Al-Enizi, “Enhanced electro-adsorption desalination performance of graphene by TiC,” *Sep Purif Technol*, vol. 254, Jan. 2021, doi: 10.1016/j.seppur.2020.117602.

[186] S. D. Datar, K. Mohanapriya, D. J. Ahirrao, and N. Jha, “Comparative study of electrosorption performance of solar reduced graphene oxide in flow-between and flow-through capacitive deionization architectures,” *Sep Purif Technol*, vol. 257, Feb. 2021, doi: 10.1016/j.seppur.2020.117972.

[187] Z. Ding, X. Xu, Y. Li, K. Wang, T. Lu, and L. Pan, “Significantly improved stability of hybrid capacitive deionization using nickel hexacyanoferrate/reduced graphene oxide cathode at low voltage operation,” *Desalination*, vol. 468, Oct. 2019, doi: 10.1016/j.desal.2019.114078.

[188] A. M. Al-Enizi, R. M. Abdel Hameed, M. M. El-Halwany, M. Bakrey, S. F. Shaikh, and A. Yousef, “Tungsten carbide@graphene nanoflakes: Preparation, characterization and electrochemical activity for capacitive deionization technology,” *J Colloid Interface Sci*, vol. 581, pp. 112–125, Jan. 2021, doi: 10.1016/j.jcis.2020.06.089.

[189] W. Dianbudiyanto and S. H. Liu, “Outstanding performance of capacitive deionization by a hierarchically porous 3D architectural graphene,” *Desalination*, vol. 468, Oct. 2019, doi: 10.1016/j.desal.2019.07.009.

[190] D. C. Han *et al.*, “High-performance capacitive deionization using nitrogen and phosphorus-doped three-dimensional graphene with tunable pore size,” *Electrochim Acta*, vol. 336, Mar. 2020, doi: 10.1016/j.electacta.2020.135639.

[191] H. Li, T. Lu, L. Pan, Y. Zhang, and Z. Sun, “Electrosorption behavior of graphene in NaCl solutions,” *J Mater Chem*, vol. 19, no. 37, pp. 6773–6779, 2009, doi: 10.1039/b907703k.

[192] X. Xu, L. Pan, Y. Liu, T. Lu, Z. Sun, and D. H. C. Chua, “Facile synthesis of novel graphene sponge for high performance capacitive deionization,” *Sci Rep*, vol. 5, Feb. 2015, doi: 10.1038/srep08458.

[193] X. Xu, Z. Sun, D. H. C. Chua, and L. Pan, “Novel nitrogen doped graphene sponge with ultrahigh capacitive deionization performance,” *Sci Rep*, vol. 5, Jun. 2015, doi: 10.1038/srep11225.